1492 *Biochemistry* **2011,** *50,* 1492–1504
DOI: 10.1021/bi1004156

BIOCHEMISTRY
including biophysical chemistry & molecular biology
Article

Gap Junction Hemichannel Interactions with Zwitterionic Lipid, Anionic Lipid, and Cholesterol: Molecular Simulation Studies

Andrew Hung and Irene Yarovsky*

Health Innovations Research Institute and School of Applied Sciences, RMIT University, GPO Box 2476, Victoria 3001, Australia

Received March 17, 2010; Revised Manuscript Received January 16, 2011

ABSTRACT: Interactions with membrane lipids can exert dramatic functional consequences on gap junction proteins. Recent experimental work has highlighted the importance of anionic lipids and cholesterol in facilitating channel activity. In this work, we have employed a coarse-grained molecular model in conjunction with molecular dynamics (MD) simulations to study the interactions between a connexin 26 (Cx26) hemichannel and a number of lipid species, including palmitoyloleoylphosphatidylcholine (POPC), anionic palmitoyloleoylphosphatidic acid (POPA), and cholesterol, in order to identify sites at the protein interface which may exhibit preferential, specific binding to these lipids, as well as determine the characteristics of these interactions. We have also employed an atomistic model of Cx26 embedded in a mixed PA/PC bilayer as a comparison and to elucidate further lipid−protein interactions. Our simulation results suggest enrichment of interfacial PA at the intracellular leaflet at high bulk PA concentrations. PC can form tight binding interactions with the hemichannel, particularly at intersubunit crevices (classical nonannular sites). In mixed bilayers, however, POPA competes with POPC for these sites, displacing the latter in some cases. While the residues responsible for interactions with PC and PA are similar, the latter exhibits a unique property of being capable of forming stable hydrophilic contacts with multiple residues spanning two different adjacent subunits at *both* leaflets of the bilayer, as opposed to POPC which can only do so at the extracellular side. These results suggest that POPA may be essential to channel function by acting as an intersubunit lipid bridge. Additionally, we propose that the compositional enrichment of POPA at the Cx26 interface may serve important roles in voltage gating. Simulation of a mixed POPC:cholesterol bilayer suggests that the hemichannel enhances the transbilayer mobility of vicinal cholesterols, increasing the likelihood of site-hopping and interleaflet flip-flop transitions.

Cellular communication is vital for the maintenance of tissue and organ homeostasis in multicellular organisms. Using this communication, cells can sense differences in environmental conditions and rapidly transmit this information to adjacent cells, enabling entire networks of interconnected cells to synchronize responses. One type of rapid communication between cells is mediated via intercellular channels that cluster in specialized regions of the plasma membrane to form gap junctions (*1*−*5*). Gap junctional channels link the cytoplasm of cells, providing a means for direct exchange of ions (K^+ and Ca^{2+}), second messengers (e.g., cAMP and inositol 1,4,5-triphosphate (IP3)), and small metabolites (e.g., glucose), thereby allowing intercellular electrical and biochemical coupling (*6*−*10*). Gap junction channels form by extracellular docking of two single membrane-spanning "hemichannels" (or "connexons"), each formed by six connexin proteins; one hemichannel is provided by each apposed cell (*11*). Nonjunctional, unpaired hemichannels in plasma membrane are also known to have regulated biological functions (*12*). To date, more than 20 different connexins have been identified in the human genome, named according to the molecular mass of the isoform (e.g., connexin 26 (Cx26) has a mass of 26 kDa). Connexons (hemichannels) may be homo- or heteromeric, and junctional channels may be formed by identical or different connexons. The diversity of connexin isoforms, as well as their different structural combinations, provides "functional tuning" of this family of membrane channels. The importance of gap junction channels is highlighted by the plethora of pathologies which are known to directly result from mutations. An example is the M34T mutation in Cx26, associated with hereditary, nonsyndromic hearing loss (*13*).

Recently, Maeda et al. (*14*) obtained the first high-resolution (3.5 Å) electron microscopy (EM) structure of a gap junction, Cx26. Each apposing hemichannel of the gap junction is a homohexamer and consists of six identical Cx26 subunits arranged in a 6-fold symmetry about a central axis, which passes through a wide pore of ∼15 Å diameter. Each of the subunits comprise four (*4*) membrane-spanning helical segments, labeled TM1−TM4,[1] connected via loops at the intracellular side and via a small β-barrel at the extracellular end. The TM1 helix contains a steep kink at the intracellular side which results in the placement of a short N-terminal segment of ∼10 residues (the "N-terminal plug") directly inside the pore, with the terminus effectively forming a pore lining.

The experimentally obtained structure of Cx26 constitutes a significant step toward understanding the properties of gap

*To whom correspondence should be addressed. E-mail: irene.yarovsky@rmit.edu.au. Phone: +61 3 9925 2571. Fax: +61 3 9925 5290.

[1]Abbreviations: CG, coarse grained; IC, intracellular; MD, molecular dynamics; PDB, Protein Data Bank; POPA, palmitoyloleoylphosphatidic acid; POPC, palmitoyloleoylphosphatidylcholine; TM, transmembrane; XC, extracellular.

 Published on Web 01/17/2011

junctions. However, for membrane proteins, interactions with membrane lipids can also have dramatic functional and structural consequences (*15*−*20*). For connexin channels this is no doubt true; lipids are likely to modulate channel function and play fundamental roles in junctional plaque structure formation and maintenance. Thus, in addition to understanding protein structure, a detailed elucidation of lipid association is also vital for a comprehensive understanding of membrane protein function. Recently, Locke et al. (*21*) have identified a number of lipids which most tightly associate with Cx26 hemichannel and gap junctions. For hemichannels, anionic lipids were found to form the most significant binding, remaining bound despite detergent washing, while no detectable traces of zwitterionic lipids (such as PC) remain associated with the protein after detergent treatment. Additionally, they identified anionic lipids and cholesterol as essential components in liposomes which sustain channel activity. Although these studies have shed light on the importance of lipids on Cx26 function, a three-dimensional channel structure of sufficient resolution to identify strongly associated membrane lipids has not yet been obtained.

Computational molecular simulations can help to bridge this crucial gap in our understanding of the properties and function of this important membrane protein. Numerous molecular dynamics (MD) simulations have been performed on membrane proteins embedded in lipid bilayers (*22*−*25*). More recent work has focused on computational studies of mixed bilayers, including anionic lipid binding to KcsA (*26*), and interactions between anionic lipids, phosphocholine, cholesterol, and the nicotinic acetylcholine receptor (nAChR) using all-atom force field methods (*27*). Differences in protein interactions and lipid conformations between phosphatidylcholine and phosphatidic acid in the vicinity of nAChR have been identified using MD (*28*). Microsecond-length atomistic simulations have been performed to identify favorable cholesterol binding sites and their structural modulatory effects on rhodopsin (*29*). Cholesterol interactions with the A(2A) receptor have also been studied by atomistic MD, suggesting a possible role for cholesterol in stabilizing a helix against structural deformation (*30*). Despite the capability for obtaining atomic resolution insights into protein−lipid interactions, all-atom MD methods are computationally expensive, making difficult the task of ensuring adequate exploration of configuration space for identifying favorable lipid interaction sites on a membrane protein surface. An alternative to atomistic MD is coarse-grained (CG) simulations, in which several atoms are represented by single interaction sites, resulting in dramatic reduction in computational overhead and enabling the study of molecular phenomena at much higher time and length scales than atomistic models(*31*−*33*). CG methods have been employed to study numerous membrane proteins. Sansom et al. has systematically catalogued a large number of CG simulations of membrane proteins and peptides of known structure (*34*, *35*). One of the most demonstrably successful CG force fields is MARTINI (*31*), which has been employed to study peptide−micelle interactions, peptide toxin self-assembly and membrane insertion, and membrane protein−lipid self-assembly (see Sansom et al. and references therein for numerous examples (*35*)). In this model, significant computational speedup is possible due to a number of factors. First, the coarse-graining scheme produces a reduction in the total number of particles, and therefore a significant reduction in the number of nonbonded interactions, in the simulation system. Second, larger simulation time steps may be used as a result of the removal of fast degrees of freedom such as individual bond length/angle vibrations and torsion angle rotations. Furthermore, there is a "smoothing" of the potential as a result of combining several atoms into single sites, which in turn produces smoother free energy landscapes which are more easily explored by unbiased simulation dynamics (in contrast to rugged, atomistic landscapes, which contain multitudes of local energy minima).

In the present work, we employ the MARTINI force field in conjunction with MD simulations to study the interactions between a Cx26 hemichannel and a number of lipid species, including phosphatidylcholine (PC), anionic phosphatidic acid (PA), and cholesterol, in order to identify sites at the protein interface which may exhibit preferential, specific binding to these lipids. We investigate the molecular level interactions between identified tight-binding lipids and residues at the protein surface which manifest persistent association with the lipids. Furthermore, we examine the effects that the presence of the hemichannel exerts on the surround lipids in terms of their dynamics and structure. To these ends, we have performed multimicrosecond long CG simulations of the hemichannel embedded in (1) a pure POPC bilayer, (2) a mixed POPC:POPA bilayer with low PA content, (3) a mixed POPC:POPA bilayer with high PA content, and (4) a mixed POPC:cholesterol bilayer. In addition, we have performed atomistic simulations of a hemichannel embedded in (1) a pure POPC bilayer and (2) a mixed POPA:POPC bilayer. Use of a combined, multiscale approach allows the exploitation of the individual advantages conferred by both types of models. The CG simulations enabled an unbiased determination of favorable lipid binding sites on the hemichannel protein. Subsequently, we used the information acquired from the CG simulations to build an atomistic model of a mixed bilayer, which enables study of specific lipid−protein interactions at the atomic level. To the best of our knowledge, the work presently described is the first computational study of a gap junction based on an experimentally determined, high-resolution structure. Earlier work performed by Fleishman et al. (*36*, *37*) employed computational methods to model Cx26 based on intermediate-resolution structures of the protein. The current work is also the first molecular level study of lipid interactions with a gap junction hemichannel protein.

METHODS

Molecular Dynamics Simulation Parameters. All MD simulations were performed using GROMACS version 3.3 (*38*−*40*) under constant particle number, pressure, and temperature (NPT) conditions. For the coarse-grained simulations, temperature coupling was maintained with a Berendsen thermostat (*41*) with a coupling constant of 40 ps and a reference temperature of 300 K. Electrostatic (Coulombic) interactions had a relative dielectric constant of 20 which was smoothly shifted to zero between 0 and 1.2 nm, and van der Waals interactions were smoothly shifted to zero between 0.9 and 1.2 nm. Each system was pressure-coupled anisotropically with a Berendsen barostat at 1 bar with a coupling constant of 40 ps and a compressibility value of 1.0×10^{-5} bar^{-1}. The time step of integration was 20 fs. Each of the four systems was simulated for 1000 ns; however, by convention, CG simulation lengths are typically quoted using their "effective" simulation times (in this case, 4 μs), which are 4-fold greater than the actual simulation length. This convention has been adopted due to the estimated 4-fold increase in configurational sampling conferred by the use of smoother CG potential as determined by the

diffusion coefficient of CG water beads (*33*). We follow this convention in subsequent discussions. For the atomistic MD simulations, the protein was modeled using the GROMOS96 force field (*38*) with the 53A6 parameter set (*42*, *43*). The POPC and POPA lipids were modeled using force field parameters derived from those of Berger et al. (*44*). The phosphate headgroup of POPA was singly protonated, producing an overall −1 charge per lipid. Temperature and pressure coupling parameters were the same as those described above for the CG simulations. Long-range electrostatic interactions were treated with particle-mesh Ewald (PME) summation (*45*). The time step for integrating the equations of motion was 2 fs. Analyses were performed using the Gromacs suite of software. Molecular graphics were acquired using VMD(*46*).

Connexin 26 Hemichannel Model Construction. We construct a hemichannel CG model based on the experimental cryoelectron microscopy structure obtained by Maeda et al. (*14*). In the most recent structure, obtained at 3.5 Å resolution, several segments are missing: the loop region at residues 110−124 and the C-terminal end of the TM4 helices comprising residues 218−226, as well as the N-terminal Met. We begin by constructing the atomistic model of the entire chain of a Cx26 subunit, repairing the missing segments using the molecular modeling tools in Deepview (*47*). This is subsequently followed by conversion to the MARTINI CG model. We first added a single Met to the N-terminus assuming α-helical backbone torsion angles. Second, the missing TM2−TM3 loop is reconstructed using the loop-building algorithm implemented in Deepview. We have selected the loop structure with the lowest predicted energy. Finally, the missing C-terminal segment of TM4 is initially assumed to adopt an α-helical structure. In order to test the stability and validity of the resultant ("repaired") model, as well as lend further guidance into the manner in which to best construct the MARTINI CG model (i.e., how to assign the backbone angle and torsion angle terms for the experimentally missing segments; described below), we have performed a 28 ns atomistic MD simulation of the Cx26 hemichannel embedded in a POPC bilayer. Following the all-atom MD simulation of Cx26 in a POPC bilayer, we find that the overall symmetry of the helix bundle is well maintained. The TM2−TM3 loop regions exhibit relatively large fluctuations. Most importantly, the C-terminal r218−226 segments of TM4 of all of the subunits rapidly lose their initially assigned α-helical structures and adopt random coil conformations (see Figure 1A). Based on our atomistic MD simulation, we assign backbone bending and torsion angle parameters for the MARTINI CG model of the protein assuming random coil structures for the TM2−TM3 loop and the TM4 C-terminus, detailed below.

Coarse-Grained Models and System Setup. We have employed the MARTINI force field (*31*) to study the interactions between lipid bilayers and a membrane-embedded Cx26 hemichannel. Specifically, we study the interactions between Cx26 and a pure POPC bilayer, mixed POPC:POPA bilayers, and a mixed POPC:cholesterol bilayer. This force field has been successfully applied in numerous studies of peptide and protein−lipid interactions (*35*) and lipid phase separation in mixed component lipid membranes (*48*, *49*). It uses a four-to-one (4−1) atom-site mapping, in which typically four (*4*) heavy atoms (i.e., atoms besides hydrogen) are represented by a single interaction site, reducing the granularity of representation of the molecule. The model takes into account four main types of interaction sites: polar (P), nonpolar (N), apolar (C), and charged (Q). For particles of type N and Q, four subtypes (0, d, a, and da) are further distinguished. Subtype 0 applies to groups in which no hydrogen-bonding capabilities exist, d and a are for groups that could act as a hydrogen bond donor or acceptor, respectively, and da is for groups with both donor and acceptor options. All nonbonded particles interact via a Lennard-Jones (LJ) potential. In addition to the LJ interaction, charged groups (type Q) interact via the normal electrostatic Coulombic potential. The particle types for most amino acids were determined by comparison between simulation results and experimental measurements of the water−oil partitioning coefficients of the amino acid analogues. Details of the assignment of particle types and coarse-grained force field parameters for amino acids can be found in ref *31*. The bonded and nonbonded parameters for POPC and cholesterol are taken from those described in Monticelli et al. (*31*). Parameters for POPA are adapted from those of POPC, i.e., identical but with a missing choline bead. The charge state of the CG POPA lipid is therefore −1 in the current simulations.

We have constructed models of the Cx26 hemichannel following the methodology prescribed by Monticelli et al. (*31*). For the protein, each amino acid is represented by a single backbone bead harmonically bonded to side chain beads. Except for glycine, all residues consist of at least one side chain bead. We assign all nonbonded interaction parameters for the amino acids according to Monticelli et al. (*31*). The peptide is composed of a series of CG residues harmonically linked via the backbone beads. In Monticelli's prescription, backbone bonded parameters are dependent on the predefined secondary structure of the residues (helix, strand, or coil). We have performed an initial test of the stability of the CG Cx26 hexamer in a (likewise CG) POPC bilayer, fully solvated, based on the values of backbone angle parameters assigned for each residue according to their secondary structure as computed using DSSP (*50*), assuming random coil structures for the TM2−TM3 loop and C-terminus of TM4. However, the symmetry of the hexamer was disrupted within ∼200 ns, with collapse and closure of the central pore (data not shown). Thus, for all of the subsequent simulations discussed in this report, we have used the experimentally derived structure of Cx26 and placed soft positional restraints on the backbone beads of all residues except for those of the TM2−TM3 loop and TM4 C-terminus, for which we allow free motion with the bending and torsion angle terms consistent with "random coil" according to the current implementation of the MARTINI force field. This enables the relaxation of the lipid bilayer around the protein. A snapshot of a subunit of the CG protein model after 4 μs simulation in a POPC bilayer is shown in Figure 1B to illustrate the flexibility of the TM4 segment.

We have performed CG simulations of four systems, each with the backbone positionally restrained Cx26 hemichannel embedded in bilayers of different compositions: pure POPC (hereafter designated as **cg-hc-POPC**), 9POPC:POPA (**cg-hc-9PCPA**), 2POPC:POPA (**cg-hc-2PCPA**), and 7POPC:cholesterol (**cg-hc-7PCCHOL**). In addition, each of the above four systems was simulated in quadruplicate (i.e., four independent simulations) with identical protein and lipid composition but with different initial lipid positions to enhance the statistical significance of the results obtained. Each simulation was set up in the following manner: first, a fully solvated bilayer, without the protein, composed of 512 lipids in total (including POPA and cholesterol) was simulated for 1600 ns. The coordinates for the four replicate simulations of each system were built by extracting frames from the protein-free lipid simulations at 400, 800, 1200,

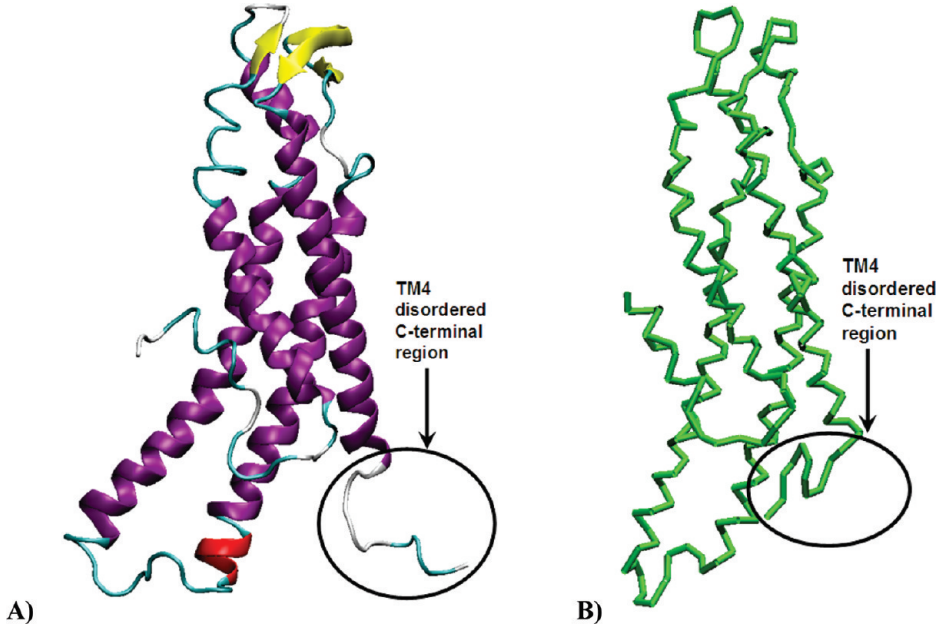

FIGURE 1: (A) Snapshot illustration of a subunit of a Cx26 hemichannel after atomistic MD simulation for 28 ns in a POPC bilayer. Protein backbones are given as ribbon representations. Note the formation of a random coil at the C-terminal end of the TM4 helix. (B) Snapshot of a coarse-grained model of a subunit after 4 μs simulation in a POPC bilayer. Only the backbone is represented. Green sticks represent bonds between backbone beads.

and 1600 ns and inserting the hemichannel into the bilayer in such a way as to ensure that the hydrophobic segments of the transmembrane domain coincide approximately with the hydrophobic core of the bilayers. Illustrations of a typical Cx26 bilayer simulation are given in Figure 2, which indicate the location of the protein relative to the phosphate beads of the lipids in the initial setup. Water beads (modeled using Pda beads) and an appropriate number of cations and anions were then added to solvate the entire system and to model ~150 mM ionic concentration, plus an additional number of cations to neutralize the simulation cell. MD simulation trajectories were then collected for these systems. Details of the simulations are in Table 1.

Atomistic Models and System Setup. We have employed atomistic models to study the interactions between a Cx26 hemichannel and its surrounding POPC and POPA lipids and compared these results with those obtained from the CG simulations. The complete protein structure was obtained by insertion of missing loops and C-terminal segment, constructed as described in the section above (coarse-grained models and setup). Two atomistic simulations were performed: (1) A Cx26 hemichannel embedded in a pure POPC bilayer, consisting of 514 lipids (hereafter designated as **aa-hc-POPC**). This system was simulated for 28 ns. (2) A Cx26 hemichannel embedded in a mixed POPA:POPC bilayer (designated **aa-hc-PCPA**), simulated for 28 ns. This system was constructed based on the information obtained from long time scale CG simulations, which indicated that POPA preferentially binds to crevices in the regions between adjacent subunits (described below; see *Nonannular Sites: Identification by Lipid Distributions*). We have therefore set up our mixed lipid simulation in such a manner as to ensure that POPA were initially located at these regions, enabling the study of lipid−protein interactions even on the relatively short time scale accessible by atomistic simulations. A graphical illustration of the initial hemichannel and POPA lipid structures is given in Supporting Information Figure S1. The membrane is composed of 12 POPA and 502 POPC, generated as follows: the 28 ns frame of the simulation trajectory of **aa-hc-POPC** was extracted, and 12 POPC lipids (6 each at the intra- and extracellular leaflets) which are tightly associated with the protein at intersubunit regions were selected and altered to POPA by replacement of cholines with protons.

RESULTS AND DISCUSSION

Annulus Size and Interfacial Lipid Compositions. We have employed CG simulations to examine the intra- and extracellular (IC and XC) compositions of lipids in direct contact with the protein (i.e., "interfacial" lipids) in comparison with the bulk. For each frame in a given simulated trajectory, a POPC or POPA is defined and counted as belonging to the protein−lipid interface if it exhibits more than ten atomic contacts within 6 Å of the protein. For cholesterol, the contact criterion is >5 contacts within 6 Å. For each Cx26 subunit, the average number of lipids of each type in contact is calculated over the final 3200 ns of the trajectory. This enables an estimate of the size and lipid composition of the annular shell for each of the simulated systems. Figure 3A shows the number of interfacial lipids (PC, PA, and cholesterol) per subunit for each simulation, with each value being an average of the trajectory averages of four replicate simulations and six subunits (with associated standard deviations as error bars), i.e., an average over 24 samples. The trajectory averaged values of interfacial lipids for each subunit and each replicate simulation are provided in Supporting Information Figure S2A−G, with error bars indicating fluctuations during the course of each simulation. We note that the fluctuations are relatively low for all of the simulated systems, with variations of between one and three lipids in each leaflet per subunit. This suggests that the lipid packing around the protein is nearly at a maximum throughout the simulations, with rapid exchange of most of the interfacial lipids at the protein surface; i.e., as a lipid leaves the interface, it is rapidly replaced by another, with a relatively short vacancy time (lipid residence times are discussed in further detail below).

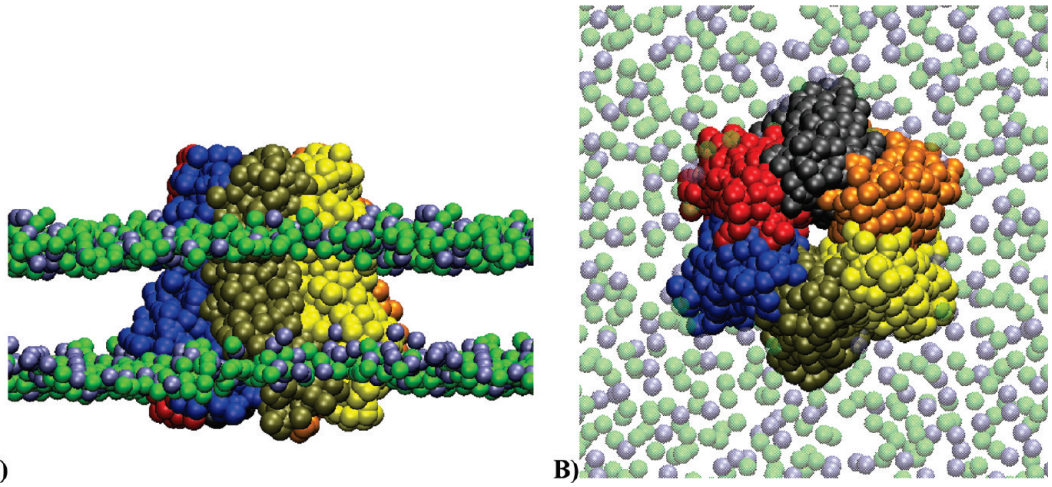

FIGURE 2: Graphical representation of the initial coarse-grained simulation setup, with a Cx26 hemichannel embedded in a bilayer composed of 262 POPC and 131 POPA lipids (corresponding to a ratio of 2POPC:POPA). View along the (A) bilayer plane and (B) *z*-axis (bilayer normal). Green spheres represent POPC phosphate beads (PO4), while light blue spheres represent POPA PO4. Water, ions, and other lipid beads are excluded for clarity.

Table 1: Details of the Four Coarse-Grained (CG) and Two All-Atom (AA) Protein Bilayer Simulation Systems[a]

	pure POPC	9POPC:POPA	2POPC:POPA	7POPC:chol
simulation labels	**cg-hc-POPC/aa-hc-POPC**	**cg-hc-9PCPA/aa-hc-PCPA**	**cg-hc-2PCPA**	**cg-hc-7PCCHOL**
no. of POPC	393, 514 AA (total) 182, 245 AA (IC) 211, 269 AA (XC)	353, 502 AA (total) 160, 239 AA (IC) 193, 263 AA (XC)	262 (total) 119 (IC) 143 (XC	308 (total) 145 (IC) 163 (XC)
no. of POPA	0	40, 12 AA (total) 22, 6 AA (IC) 18, 6 AA (XC)	131 (total) 63 (IC) 68 (XC)	0
no. of CHOL	0	0	0	47 (total) 21 (IC) 26 (XC)
no. of water	20234, 50357 AA	20194, 50357 AA	20103	19563
no. of ions	300 Na^+, 354 Cl^-	340 Na^+, 354 Cl^- 352, 354 AA	431 Na^+, 354 Cl^-	300 Na^+, 354 Cl^-
simulation time (ns)	4000 (28 AA)	4000 (28 AA)	4000	4000

[a]Data corresponding to the atomistic simulations are indicated by "AA". Each CG system was simulated in quadruplicate.

In all of the systems, there are more interfacial lipids at the IC leaflet. For **cg-hc-POPC** (single component POPC bilayer), there are 6.20 ± 0.26 per subunit at the IC side, with 5.50 ± 0.19 at the XC side; similar values are obtained for **cg-hc-9PCPA** (IC = 6.33 ± 0.35, XC = 5.38 ± 0.15), **cg-hc-2PCPA** (IC = 6.47 ± 0.34, XC = 5.40 ± 0.16), and **cg-hc-7PCCHOL** (IC = 6.66 ± 0.37, XC = 5.27 ± 0.19). The relatively larger size of the IC lipid annulus is consistent with the morphology of the hemichannel. Toward the XC side, the protein consists of a more tightly packed helical bundle with narrow dimensions, with a subsequently lower lipid-exposed surface, while the hexamer is wider toward the IC side due to the tilt of the outer (TM3/TM4) helices, resulting in the presentation of a higher lipid-exposed surface. For both **cg-hc-9PCPA** and **cg-hc-2PCPA**, the number of interfacial PA is substantially higher at the IC leaflet, while the numbers of PC are approximately equal at both leaflets. This suggests the displacement of interfacial PC by PA at the IC leaflet. In contrast, while there is also a greater number of interfacial cholesterols at the IC leaflet, their presence does not shift the relative proportion of IC and XC interfacial PC. This suggests that, unlike PA (which has similar dimensions as PC), cholesterols do not displace PC in order to form contacts with the protein. Rather, due to their small size and planar dimensions, cholesterols can contact the protein surface alongside PC. We quantify the relative preference of the protein for interactions with different lipid types below.

Specific interactions between the protein and lipids may result in the enrichment/depletion in concentration (relative to the bulk) of selected lipid types at the interface. The annular shell surrounding a membrane protein may therefore possess a lipid composition distinct from that of the bulk of the bilayer, and this may have important consequences for protein structure and function. Figure 3B shows bar charts of the IC and XC interfacial lipid compositions divided by their bulk values (bulk compositions are determined by the relative proportions of the total number of PC, PA, and cholesterols at the IC and XC leaflets in the simulation setups; see Table 1). Composition ratio values > 1.00 indicate *enrichment* at the interface, while values < 1.00 indicate *depletion*. Bar charts for each individual subunit and replicate simulation are shown for reference in Supporting Information Figure S3A−C. For **cg-hc-9PCPA**, the composition of interfacial POPA is enhanced at the IC side (interface:bulk composition ratio = 1.13 ± 0.07) and depleted at the XC side (0.97 ± 0.03). The relatively large uncertainties, however, suggest that the differences are marginal. In particular, the XC PA composition is similar to the bulk. PA enrichment at the IC leaflet is consistent with the higher numbers of basic residues

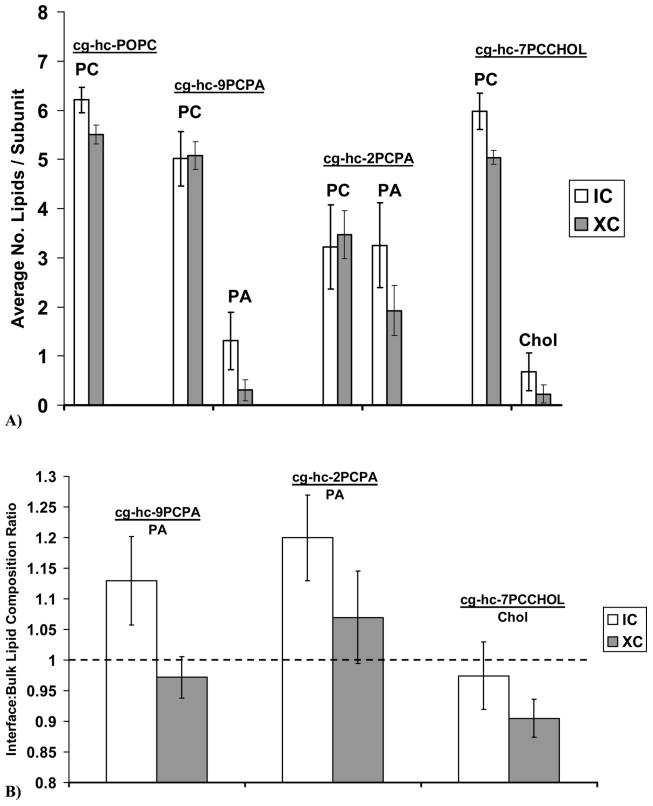

FIGURE 3: Bar charts of (A) average numbers of PC, PA, or cholesterols with > 10 (5 for chol) contacts within 6 Å for all four systems at the IC and XC leaflets (labeled in chart) and (B) interface:bulk lipid composition ratios (taking into account subunits which make > 0.4 contact for **9PCPA** and > 1.2 contacts for **2PCPA**). Averages and standard deviations (error bars) for these charts are taken over the trajectory-averaged values for six subunits in four replicate simulations.

there compared to other regions of the hemichannel and suggests that the protein selectively "picks out" POPA from the lipid milieu, increasing its effective concentration at the protein surface. For **cg-hc-2PCPA**, which has a much higher bulk POPA composition, PA is enhanced at both IC (1.20 ± 0.07) and XC (1.07 ± 0.08) sides, although only marginally for the latter. These values are both higher than those of **cg-hc-9PCPA**. Thus, a higher concentration of POPA in the membrane results in a substantial increase in Cx26 interfacial POPA enrichment, with the effect more pronounced at the IC leaflet. This may be due to the fact that at higher PA bulk concentration there is correspondingly greater mutual repulsion between these anionic lipids in the bulk. In order to escape the electrostatically repulsive environment of the bulk, the POPA preferentially binds to electrostatically attractive regions of the Cx26 hemichannel, especially at the IC side, which is rich in basic residues. We note that the orientation of Cx26 appears to conform to the "positive-inside" rule of membrane protein topology, which dictates that loops outside the membrane which are enriched in basic residues tend to reside at the cytoplasmic region due to the asymmetric distribution of anionic lipids in biological membranes (*51*). The positive-inside rule is likely responsible for the IC leaflet-biased preference for anionic lipids for Cx26.

Examination of the lipid stoichiometry for the **cg-hc-7PCCHOL** simulations shows depletion at both leaflets (IC = 0.97 ± 0.06, XC = 0.91 ± 0.03), especially at the XC. This result is in qualitative agreement with the (atomistic) simulation of nAChR described by Cheng et al. (*27*), who likewise found a depletion of cholesterol at the receptor interface relative to the bulk. However, our result indicates a preference of cholesterol for forming contacts with the IC side of the protein, similar to POPA (Figure 3A). The observed relative reduction in cholesterol percentage at the interface suggests that the protein does not selectively "pick out" cholesterol molecules from the membrane and then strongly bind them (as appears to be the case for POPA); indeed, our results suggest that there is a degree of repulsion between Cx26 and cholesterol. This lends support to the notion that changes in connexin hemichannel conductivity with respect to cholesterol concentration are due primarily to indirect (membrane-delocalized) effects (*21*), such as alterations of membrane fluidity, thickness, or lipid chain ordering. These effects indirectly modulate protein dynamics. Nevertheless, possible functional effects of direct cholesterol binding to the hemichannel cannot yet be discounted. In the following sections, we examine and identify sites at the protein surface which form favorable persistent interactions with POPC and POPA as well as cholesterol.

Nonannular Sites: Identification by Lipid Distributions. We have determined the sites at the protein surface which form favorable binding pockets for lipids and cholesterol, as well as identified the lipids involved, and have scrutinized some of their atomic level interactions with the protein. Figure 4 shows graphical representations of the protein backbone, shown as green and yellow sticks (the subunits are shown in alternating colors to allow easy identification of separate subunits and their boundaries). Also shown are selected "beads" of the surrounding lipids within 5 Å of the protein given as blue or red dots (phosphate "PO4" beads for POPC (blue) and POPA (red) and the alcohol "ROH" group for cholesterol (red)). Each dot, representing one of the lipid beads, indicates the position of the respective lipid at one simulation time frame. The multitudes of dots in panels A−E of Figure 4 ("dot plots") indicate the positions of the selected lipid beads over time frames within the final 400 ns of simulations for all four of the systems. In these figures, we interpret regions of concentrated lipid dots as being indicative of tight binding between the protein and the lipid. We note that Figure 4 displays results obtained for one replicate simulation for each of the systems. Similar tight binding sites for both POPC and POPA are obtained for all of the replicate simulations, as illustrated by the dot plots of replicate **cg-hc-POPC** and **cg-hc-2PCPA** simulations in Supporting Information Figures S4 and S5, respectively.

For the **cg-hc-POPC** simulation, the dot plots for interfacial POPC lipids at the IC and XC leaflets are shown in panels A and B of Figure 4, respectively. It can be seen that POPC forms contacts all around the hemichannel at both leaflets. However, at the intracellular side, approximately 20 distinct sites can be identified in which the lipid appears especially immobile, each of these sites being characterized by a tight cluster of blue dots. A similar number of clusters can be seen at the extracellular side (Figure 4B). Lipids at these sites are strongly bound and exhibit limited diffusion, as confirmed by visual inspection of the trajectory. We note that the majority of these sites are located at intersubunit crevices for both leaflets. Thus, we hereafter refer to such sites as nonannular, which conventionally refer to nAChR interhelix and intersubunit crevices in which lipids are believed to be strongly bound and exhibit motional restriction, as well as adopt structural features different from those of bulk lipids (*15*, *52*−*56*). However, our current CG simulations suggest that nonannular sites also exist for connexin hemichannels, which

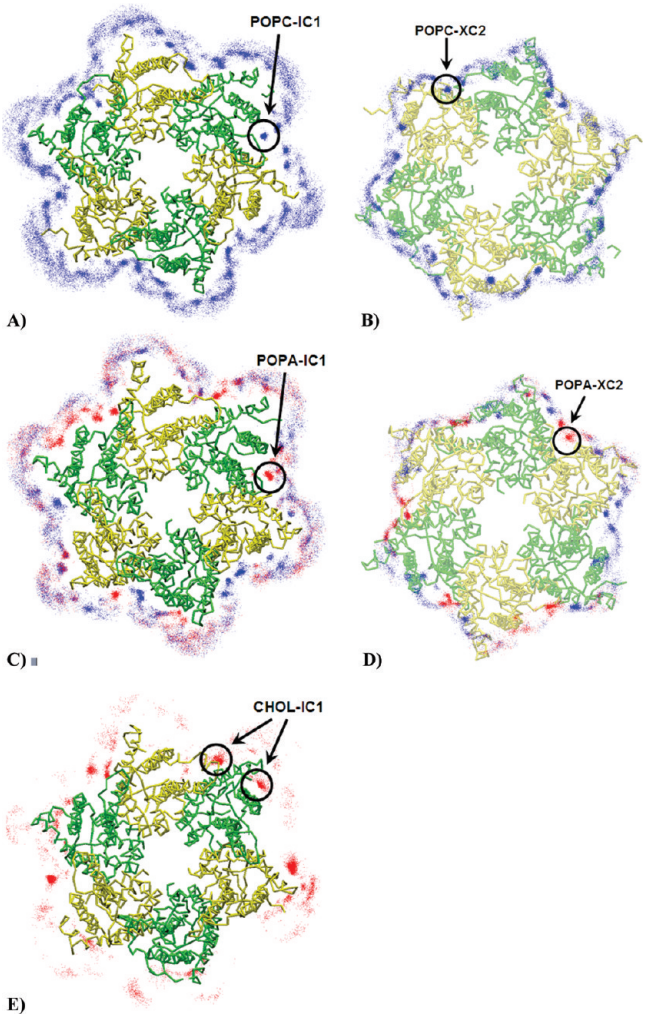

FIGURE 4: Graphical representations of Cx26, viewed along bilayer normal (except for F), with surrounding dots representing PC/PA PO4 beads (blue and red, respectively) and cholesterol ROH beads (red). Each dot represents the position of the lipid at a certain time frame within the final 400 ns of simulation. (A) Intracellular (IC) and (B) extracellular side for the POPC simulation. (C) IC and (D) XC sides for the 2POPC:POPA simulation and (E) IC side for the POPC:chol simulation, viewed along bilayer normal.

may furthermore suggest that the special preference of intersubunit crevices for strong lipid binding may be a general feature of all membrane proteins with α-helical transmembrane domains. The validity of this hypothesis requires further experimental and computational studies of membrane proteins in lipid bilayers. Furthermore, although the experiments of Locke et al. (*21*) did not identify PC among lipids that remain bound to Cx26 after extensive washing with detergent buffers, they did not rule out the possibility that PC may form specific interactions with the protein (albeit likely to be much weaker than those of the anionic lipids, which were present after detergent treatment). Our current simulations suggest that sites may exist on the protein surface that allows tight binding to PC lipids.

We have similarly examined the **cg-hc-2PCPA** simulation dot plots (Figure 4C,D) to identify favorable binding sites for POPA, indicated as red dots. On both the intra- and extracellular sides, we find that both POPC and POPA form clusters at hemichannel nonannular sites. Inspection of the intracellular side suggests that three such sites are largely occupied by POPA, two are largely occupied by POPC, and others involve a combination of tight occupancies by both lipids. At the extracellular side, four nonannular sites are occupied by POPA, one by POPC, and one by both. Thus, it appears that POPA competes with POPC in occupation of nonannular sites located at intersubunit regions, displacing POPC completely at some sites while sharing occupancy at others.

Figure 4E illustrates favorable binding sites for cholesterol, as obtained from our **cg-hc-7PCCHOL** simulations. The advantage of using CG models is that natural diffusion of cholesterol into gaps in the protein can be examined within a reasonable computation time, a phenomenon which may not be easily observable using atomistic simulations (*27*). In our current simulation, examination of the dot plot for cholesterol on the IC side reveals several possible tight-binding sites, with two intersubunit crevice locations and three other possible binding sites in the vicinity of the exposed M4 helices. Owing to the simple structure of cholesterol, examination of a (nonannular) cholesterol reveals relatively simple interactions with the protein, with single persistent interactions of the alcohol ROH group with a hydrophilic side chain such as Ser or Thr, and hydrophobic interactions via its ringed structure with hydrophobic residues on the protein deeper inside the bilayer.

Nonannular Sites and Lipid Binding Lifetimes. In order to quantify the kinetics of the interactions between the lipids and the hemichannel, and to determine the extent to which our simulations were of sufficient length to sample the range of possible lipid−protein interactions (of differing persistence), we have characterized the lifetimes of lipid−protein contacts for all of the simulated systems as follows. We also identify the residues which are responsible for persistent interactions between the protein and PC or PA. In a given simulation, for each lipid, we calculate the maximum continuous stretch of time for which the center of mass (COM) of that lipid lies within 40 Å of the COM of the hemichannel (test calculations have shown that >10 lipid−protein contacts within 6 Å are required to satisfy this condition). This time value constitutes the "contact lifetime" for the respective lipid. Subsequently, contact lifetimes were calculated for all lipids in each simulation, and a histogram was constructed. Histograms describing the number of lipids with a given protein contact lifetime are given in Figure 5. The contact lifetime histogram for **cg-hc-POPC** is shown in Figure 5A. We note that *all* of the lipids (in all of the simulations) exhibited finite contact lifetimes, indicating that the simulations are of sufficient length to enable each lipid to diffuse along the bilayer plane and encounter the hemichannel at least once. Furthermore, at both leaflets, there are lipids which interact with the protein with residence times spanning the entire range of possible values (i.e., up to 4000 ns), indicating that the simulation time was sufficient to allow the lipids to sample a large number of interaction sites/types. The persistence of lipid−protein contacts may be approximately divided into three categories. First, the vast majority of the lipids exhibit relatively low lifetimes (<600 ns), indicative of transient interactions which do not result in persistent contacts with the protein. Second, some of the lipids exhibit higher contact lifetimes, between 600 and 1500 ns. These correspond to the lipids which remain at the protein surface and undergo diffusion along the surface without becoming "trapped" at particular, tight-binding sites (i.e., annular lipids). These lipids are characterized by "dots" which appear in more diffuse clusters around the protein surface in Figure 4. Third, lipids which exhibit lifetimes >1500 ns are those located at intersubunit crevice regions (corresponding to those represented by dots in tight clusters

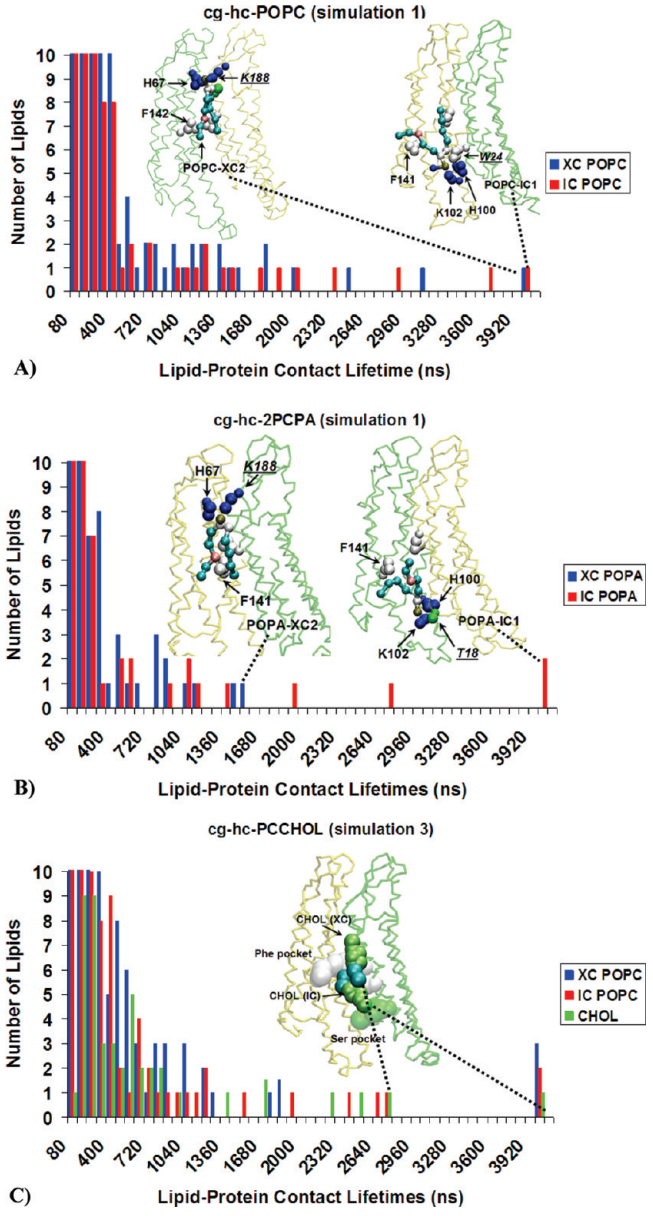

FIGURE 5: Histograms of lipid−protein contact lifetimes calculated over the entire course of each simulation trajectory for (A) **cg-hc-POPC**, (B) **cg-hc-2PCPA**, and (C) **cg-hc-PCCHOL**. The *y*-axes are truncated at 10 to ensure visibility of the bars for high lifetime lipids. Molecular graphics inserts illustrate the binding positions and key interactions between the hemichannel surface and selected lipids/cholesterols with high protein contact lifetimes.

shown in Figure 4), which are tightly bound and do not readily diffuse away from their binding sites. (i.e., nonannular lipids). For **cg-hc-POPC**, the histogram shows that roughly equal numbers of tightly bound lipids are found at each leaflet side. We note that a small number of these lipids have lifetimes of 4000 ns, indicating that they were initially at a nonannular site at the start of the simulation and remained there for the duration. While the possibility of a simulation artifact resulting from initial lipid placement cannot be ruled out, we note that such lipids also exist in *all* replicate simulations (see Supporting Information, Figures S4−S7), which have different initial lipid positions. Thus, rather than an artifact owing to initial condition dependence, the appearance of similar tight-binding sites in all replicate simulations suggests that these sites are genuine features of the hemichannel.

We have identified the specific lipid−protein interaction requirements for a POPC lipid to form high-persistence interactions with the protein at nonannular sites. We have selected as an illustration two particular nonannular lipids at the intra- and extracellular leaflets, shown as insets in Figure 5A (and also circled in panels A and B of Figure 4, respectively), and have identified their persistent interactions with the protein throughout the final 400 ns of the simulated trajectory. Similar interactions are identified for other nonannular lipids (not shown). A snapshot of a tight-binding POPC at the intracellular leaflet is shown in the RHS inset in Figure 5A, labeled as "POPC-IC1". The lipid is located between two subunits, with its headgroup approximately level with the loop (comprising Lys15−Ile20) which connects the M1 helix with the N-terminal plug. Its phosphate PO4 bead forms persistent electrostatic interactions with Lys102 and hydrophilic interactions with His100. Although the headgroup forms multiple simultaneous interactions with hydrophilic and charged side chains, these interactions are localized to one subunit only. In contrast, the hydrocarbon tails of the lipid form contacts with multiple hydrophobic resides of the protein from *both* subunits, especially the aromatics (Phe141 and Trp24 are shown as examples in Figure 5A). Additionally, throughout this segment of the trajectory, a single hydrocarbon chain buries deeply into the intersubunit crevice lined by hydrophobic side chains.

At the XC side (LHS of inset, Figure 5A), we find that hydrophilic interactions are formed with the lipid headgroup ("POPC-XC2") to side chains contributed from *both* neighboring subunits, with His67 contributed from one subunit and Lys188 contributed from the other. The lipid thus forms "molecular glue" that may help to hold the subunits together. POPC-XC2 also forms hydrophobic interactions via its hydrocarbon chains to aromatic (and other hydrophobic residues) contributed from both subunits, analogous to POPC-IC1 described above. However, in contrast to POPC-IC1, the extracellular nonannular POPC lipids are not able to bury deeply into the intersubunit crevice, due to the lower separation between the subunits at the extracellular side. Taken together, inspection of the specific interactions between the two long lifetime lipids and the protein revealed that, to be "captured" at a nonannular site, a POPC lipid must (1) sample an intersubunit binding site during its travels, (2) form persistent contacts with multiple polar side chains, via its phosphate, and (3) form stabilizing hydrophobic contacts with aromatic side chains via at least one of its tails.

Contact lifetime histograms of POPA−protein contacts for the **cg-hc-2PCPA** simulation are shown in Figure 5B. Inspection of the histograms for the POPC lipids in these simulations reveals very similar patterns of interactions as those for **cg-hc-POPC** discussed above; thus, we presently focus our discussion on POPA. As with POPC, the POPA lipids which exhibit long lifetime contacts (>1500 ns) reside at intersubunit crevices. Interestingly, the average nonannular POPA contact lifetime is significantly higher at the IC side, as also observed for all of the replicate simulations, as well as **cg-hc-9PCPA** (Supporting Information Figure S7A−D). This is consistent with the observation (discussed in *Annulus Size and Interfacial Lipid Compositions*) that anionic lipids form much greater numbers of contacts (primarily via phosphate interactions) at the cytoplasmic side of the hemichannel. While this asymmetry exists for POPC also, it is more pronounced for POPA. Inspection of the POPA which exhibit the longest contact lifetimes at both the XC and IC sides reveals that the anionic lipid must meet similar requirements (with

respect to specific contacts with the protein) to those of POPC for persistent binding to nonannular sites. These are shown in the graphical insets in Figure 5B. Analogous to IC nonannular POPC, POPA-IC1 (RHS inset) forms associations with hydrophilic side chains (Lys102 and His100, from the same subunit) which persist throughout the simulation. However, in addition to same-subunit contacts, this lipid also maintains tight association with Thr18 from a neighboring subunit. Thus, in contrast to POPC, a POPA at the crevice can form interactions via its phosphate headgroup that "bridge" adjacent subunits, possibly owing to its strong charge and relatively small size (choline absent). Both lipid chains are in close association with the protein surface, forming stable hydrophobic contacts with residues such as Phe141, with the unsaturated chain filling the gap between the subunits. At the XC side (LHS inset), POPA-XC2 is able to form multiple simultaneous interactions that span two adjacent subunits (His67 of one subunit, Lys188 of the other), as well as hydrophobic contacts via its hydrocarbon tails. Thus, at the XC side, nonannular POPA behaves similarly to POPC.

We have calculated protein contact lifetimes for each cholesterol in each of the four replicate simulations. In three of the replicate simulations, relatively few long lifetime cholesterols were identified (being >2000 ns), but none were as long-lived as those of POPC (Supporting Information). Interestingly, in one of the simulations (designated simulation 3), we identified cholesterols which make persistent contact with the protein with lifetimes similar to that of POPC. The contact lifetime histogram for this simulation is given in Figure 5C, with the most persistent cholesterols shown as graphical insets in the figure. The cholesterol with the longest lifetime binds to the intracellular side of the protein, at an intersubunit crevice (labeled as CHOL(IC)). Its endurance in this binding site throughout the simulation appears to be due to multiple close contacts of its ring with a cluster of Phe side chains deep in the bilayer core, as well as contacts of its hydrophilic "tail" with a cluster of Ser residues toward the intracellular side. These clusters anchor the cholesterol in place and may be identified as a possible specific interaction site for cholesterol. However, as evidenced by the rarity of very long lifetime cholesterol interactions, these sites are difficult to access or are preferentially occupied by POPC. Additionally, we identified another cholesterol which also binds persistently to the protein, at the XC side (labeled CHOL(XC) in the inset). This cholesterol also forms numerous close contacts with the Phe cluster; the binding site for this cholesterol thus partially overlaps that for the CHOL(IC) molecule. We note that these two cholesterols bind simultaneously for $>70\%$ of the trajectory. It is thus possible that the appearance of especially long contact lifetime interactions between the protein and cholesterol may be partly due to cooperative binding of two cholesterols in close proximity on the protein surface.

Connexon-Induced Cholesterol Flip-Flop. Unlike POPC and POPA, which binds tightly to the hemichannel, cholesterol in general does not remain statically bound. Rather, they exhibit a wider range of dynamics in the vicinity of the protein surface. Figure 6A shows the distribution of the hydrophilic ROH group of cholesterol during the course of a simulation (similar results are obtained for all four replicate simulations). The presence of numerous red dots in the membrane center is indicative of frequent excursions of cholesterol deep into the hydrophobic core of the bilayer. This is especially prevalent near the protein (clusters circled in the figure). This distribution pattern suggests that throughout the simulation there is significant flexibility in

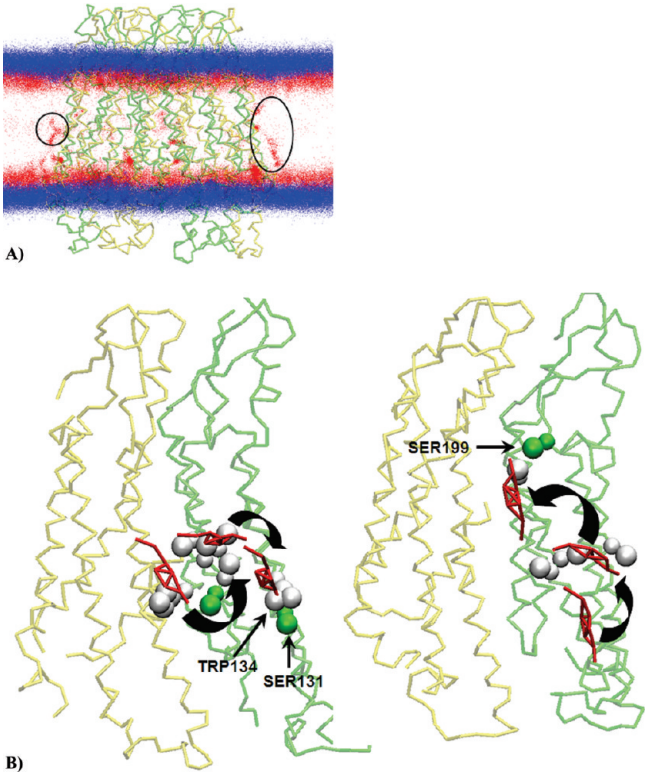

FIGURE 6: (A) Graphical representations of Cx26 viewed along bilayer plane with cholesterol ROH beads (red dots) over the final 400 ns of the **cg-hc-PCCHOL** simulation. (B) Snapshot illustrations of selected cholesterol molecules obtained from cg-hc-PCCHOL simulation, indicating cholesterol dynamics at the protein surface, with a site-hopping transition at the IC side (left) and a protein-mediated flip-flop from IC to the XC leaflet (right).

the orientation of cholesterol molecules with respect to the bilayer. Visual inspection of the trajectory confirms that cholesterol molecules, while largely maintaining an upright orientation with respect to the membrane normal, nonetheless frequently (but transiently) adopt diagonal or horizontal orientations. The presence of dense clusters of cholesterol ROH groups within the bilayer core near the protein furthermore suggests that the variation in cholesterol orientation is likely a result of interactions with the hemichannel. The protein also promotes "flip-flop" motions for some cholesterols in its vicinity, which involve the transition of a cholesterol which originally resided in one leaflet to the opposing bilayer leaflet (we note that no flip-flop transitions were observed for POPC or POPA in any of our simulations). Direct examination of some of the tight-binding cholesterol molecules sheds further light on the influence of the protein.

First, we have selected CHOL-IC1 as an illustration of the dynamic behavior of cholesterols in tight-binding (but not nonannular) sites, circled in Figure 4E. Both of the circled clusters correspond to the same cholesterol molecule, which is observed to "jump" from one binding site to the other within a short time (less than 100 ns). Figure 6B (LHS) shows three snapshots of the binding site transitions of CHOL-IC1. This cholesterol starts off from an initial site near the intersubunit crevice (at 3600 ns), with persistent interactions with a Thr side chain via its ROH group, and its hydrophobic ring structure in contact with aromatic residues of the protein. It makes an abrupt transition to a metastable position at ~3700 ns, oriented parallel to the bilayer plane and transiently stabilized by mixed

hydrophobic/hydrophilic contacts with side chains such as Trp134; this configuration remains only until ~3760 ns, after which CHOL-IC1 flips back toward a parallel orientation with respect to the bilayer normal and is stabilized by interactions with Ser131 and several hydrophobic side chains, with interactions solely with the TM3 and TM4 helices of a single subunit. Second, we have selected the sole tight-binding cholesterol on the extracellular side, CHOL-XC2, to illustrate the promotion of cholesterol flip-flop transitions due to the presence of Cx26. Snapshots are shown in Figure 6B (RHS). CHOL-XC2 initially starts off in the intracellular leaflet at ~3000 ns, with no close contacts with the protein. Upon contact with the protein at ~3500 ns, however, it abruptly adopts a parallel orientation, with stabilizing contacts with Trp134 and other hydrophobic residues. At ~3600 ns, it completes the flip-flop motion, adopting a parallel orientation with respect to the bilayer normal, ending up on the extracellular side, and forming persistent interactions with Ser199 via its ROH bead. Our results are consistent with the CG simulations of Bennett et al. (*57*), who found that cholesterol flip-flop transitions in bilayers are fast on physiological time scales. Furthermore, our simulations show that a membrane protein may further enhance flip-flop rates of cholesterol molecules in its vicinity.

Lipid-Exposed Residues and Interactions with Lipid Functional Groups. We have identified the residues which make contact with the various lipid moieties of POPC and POPA, namely, phosphate, glycerol, and hydrophobic chains, at both leaflets. These analyses enable us to identify residues which make substantial contribution to lipid interactions and which may therefore be of functional significance. The contributions of individual amino acids to gap junction formation and function are complex and currently not well understood. However, the identification of lipid-exposed residues suggests the possibility that influences on (disruptions of) Cx26−lipid interactions may partially contribute to the biochemical and biophysical consequences of mutation of these residues.

Supporting Information Figure S8A−F shows bar charts indicating the number of contacts between each residue (shown on the *x*-axis) and lipid functional groups, averaged over all subunits in all replicate simulations (i.e., 24 samples) over the final 3200 ns. A residue and lipid moiety are considered in contact if any of their CG beads are within 6 Å of each other. The residues are divided into those that reside on the IC and XC leaflets, as indicated on each chart, and sorted from left to right in order of increasing value along the *z*-axis (i.e., from IC to XC along the bilayer normal). We note that, generally, the results for PA are qualitatively similar to those of PC.

We first compare the phosphate contact profiles for PC and PA. For **cg-hc-POPC** (phosphates, Supporting Information Figure S8A), Arg216 makes the most substantial number of contacts with PC phosphates, with an average 3.08 ± 0.21 contacts. This large number is likely owing to the relatively large size of the Arg side chain, represented by two CG beads. At the XC side, His67 makes the most substantial contacts, with 1.84 ± 0.35. His67 is also identified as a tight-binding site for PC and PA, as discussed in *Nonannular Sites and Lipid Binding Lifetimes* above. Arg216 and His67 are predicted to be especially prone to attractive interaction with PC and PA phosphates and may play important roles in Cx26−membrane interactions. Currently, there are no known mutations of these residues with clinical manifestations, nor have the biochemical/biophysical consequences of their mutations or deletions been elucidated experimentally. We note, however, that although His67 and Arg216 mutations have not been studied directly, mutations of their *neighboring* residues have been studied; the Asp66His and Leu214Pro mutants are known to result in failure of gap junction formation, and Arg127His results in impaired biochemical coupling; we refer interested readers to the exhaustive compilation of gap junction mutants in Dinh et al. (*58*) and references therein. It is possible that mutations in the neighborhood of residues which form strong associations with lipid headgroups may also influence their lipid-binding propensities, which may in turn have structural and functional consequences for hemichannel and gap junction formation.

Excluding the outlier Arg216 at the IC side, the average number of contacts per residue at the IC side is 0.66 ± 0.34 and for the XC side is 0.67 ± 0.45. Thus, for PC, the number of phosphates *per residue* is generally approximately symmetric with respect to bilayer leaflet, although there are more phosphate-exposed residues at the IC side. Similar results are obtained for PA in **cg-hc-2PCPA** (Supporting Information Figure S8B). Arg216 also forms the highest number of phosphate contacts, with 1.65 ± 0.26 contacts. His67 is also among the most significant residues at the XC side (0.55 ± 0.21). Similar to PC, there is also a greater *number* of phosphate-exposed residues at the IC side. However, in contrast to PC, there is substantial leaflet asymmetry in the phosphate contacts *per residue*, with IC = 0.54 ± 0.28 (excluding Arg216) and XC = 0.31 ± 0.16. This is indicative of stronger overall association between the IC side of the protein and PA phosphates compared to the XC side. Functional effects imparted by PA owing to phosphates are therefore likely to be mainly mediated at the intracellular side. This is consistent with the well-established observation that anionic lipids are predominantly located in IC leaflets of eukaryotic cells (*59*).

The glycerol contact profiles for PC and PA are shown in Supporting Information Figure S8C and Figure S8D, respectively. Trp134 forms the highest number of contacts with both PC and PA glycerols (4.82 ± 0.51 and 2.62 ± 0.46, respectively). There are also no known clinically relevant mutants for this residue nor direct experimental investigations of its mutations. Nonetheless, the biophysical effects of mutations of residues near Trp134 have been characterized: Thr135Ala results in nonfunctional gap junctions, while Tyr136X results in failure of gap junction formation. Tyr212 also forms substantial numbers of contacts with both PC and PA (3.13 ± 0.59 and 1.42 ± 0.37, respectively). In the vicinity of Tyr212, the Leu214Pro mutant is also known to prevent gap junction formation. For PA, Ile20 forms the most significant number of glycerol contacts (after Trp134, with 1.74 ± 0.49). The Ile20Thr mutation is known to disrupt junction formation, while Ser19Thr results in reduced cellular biochemical coupling.

Excluding the outlier Trp134, we compare the average glycerol contact *per residue* at the IC and XC sides for PC and PA. Similar to phosphate contacts, we find that there is a moderate bias toward higher glycerol contact *per residue* at the IC side for POPA (IC = 0.64 ± 0.47, XC = 0.57 ± 0.24). There is a slight bias toward the XC side for POPC (IC = 1.00 ± 0.93, XC = 1.20 ± 0.75). However, given the relatively high uncertainties, per residue glycerol contact leaflet asymmetry is far less pronounced for glycerols compared to phosphates.

Based on the results discussed above, Arg216 and Trp134 are identified as residues which make the highest contacts with phosphates and glycerols, respectively. Together with residues at nonannular sites discussed above, it is possible that mutations

of these residues may cause a reduction in the propensity of Cx26 to interact with lipids, with possible biophysical and functional implications. It may also be of interest to experimentally determine the effects of mutation or deletion of other lipid-exposed residues.

Lipid tail contact profiles for PC and PA are given in Supporting Information Figure S8E and Figure S8F, respectively. Aromatic residues make the most marked numbers of contacts with lipid chains, with Trp24, Trp134, Phe141, and Phe142 being the principal contact residues for both PC and PA. Tyr152 is also especially prominent for PC (Supporting Information Figure S8E). Unlike the headgroup contact profiles discussed above, there are approximately equal numbers of tail-exposed residues at both leaflets and no significant asymmetry in tail contacts per residue with respect to leaflet for PC (IC = 2.89 ± 2.74, XC = 2.88 ± 2.85) nor PA (IC = 1.49 ± 1.45, XC = 1.27 ± 0.84). However, there are higher numbers of contacts with aromatic residues at the IC leaflet.

Atomistic Simulations and Comparisons with CG Model. We have employed atomistic simulations (using the GROMOS96 force field) to study interactions between POPC, POPA, and Cx26. This enables comparisons with the CG simulations to determine the extent to which simplified molecular representations can model protein−lipid interactions, as well as identify further interactions. Analyses of POPC−Cx26 interactions are based on simulation **aa-hc-POPC**, with the protein embedded in a pure POPC bilayer, while analyses of POPA−Cx26 interactions are based on simulation **aa-hc-PCPA**, with the protein embedded in a mixed PC:PA bilayer with the PA at low concentration (12 PA to 502 PC). For **aa-hc-PCPA**, the PA lipids were initially placed at intersubunit crevices. This choice is based on the CG simulation results discussed above, which indicate that PA preferentially accumulates at intersubunit regions in mixed PC: low concentration PA bilayers. In particular, we identify the residues which are exposed to different lipid functional groups, delineated into IC and XC contributions, and compare these results with those acquired using CG simulations discussed above.

Supporting Information Figure S9A−F shows bar charts of contacts for each lipid-exposed residue taken as an average over the six subunits, over the final 6 ns of simulation **aa-hc-POPC**. For the atomistic simulations, two atoms are considered in contact if they are within 4.5 Å of each other. We find similar qualitative trends for the atomistic simulations compared to those of the CG simulations. We first consider phosphate interactions. For POPC (Supporting Information Figure S9A), the most significant contacts are made with residues at the IC side, namely, Lys221, His94, and Arg216, the latter also identified as an important headgroup-exposed residue from the CG simulations (cf. Supporting Information Figure S8A). There are a larger number of phosphate-exposed residues at the IC leaflet, in agreement with the CG simulations. The IC side residues exhibit moderately higher contacts *per residue*, with 5.07 ± 3.37 compared to 4.07 ± 3.26 at the XC side, although considering the size of the error bars, this apparent leaflet asymmetry is insubstantial.

For POPA (Supporting Information Figure S9B), the most significant phosphate contacts are made by Arg98, Tyr97, and His94. The latter residue at one of the subunits maintains persistent hydrogen bonding with a PA phosphate throughout the course of the **aa-hc-PCPA** simulation (>60% of the trajectory) together with Trp24 (which H-bonds to glycerol; see below) on an adjacent subunit. This is illustrated in the graphical inset in Supporting Information Figure S9A. Thus, POPA is capable of forming not only multiple simultaneous close contacts with adjacent subunits (indicated by our CG simulations) but also multiple hydrogen bonds between two adjacent subunits, which was not observed for POPC. These findings indicate that one mechanism by which POPA (and perhaps other anionic lipids) supports Cx26 channel activity involves acting as a mediative linker which binds the protein subunits together (particularly at the IC end), allowing them to couple structurally as well as dynamically. Anionic lipid-dependent intersubunit coupling may be essential to concerted motions between the protein monomers which are required for channel gating. Additionally, as with POPC, there is a higher number of PA phosphate-exposed residues at the IC leaflet. The IC side residues also exhibit moderately higher average phosphate contacts *per residue* (2.66 ± 1.83 compared to XC = 2.24 ± 0.62).

For POPC glycerol contacts (Supporting Information Figure S9C), Arg216 and Trp134 are identified as forming high numbers of contacts at the IC side, and Tyr152 at the XC side, in good agreement with CG simulations (cf. Supporting Information Figure S8C). Of particular interest is Trp134, which on one of the subunits forms the most persistent hydrogen bonding with a POPC (via glycerol) during **aa-hc-POPC** (see graphical inset). Although there are more IC glycerol contact residues, the contacts *per residue* are approximately equal between the leaflets (6.42 ± 5.34 compared to XC = 6.52 ± 7.14). For POPA (Supporting Information Figure S9D), Arg98, His94, and Trp24 form high glycerol contact numbers. The latter two from adjacent subunits both form persistent hydrogen-bonding interactions with a single PA, forming a cross-subunit lipid bridge (see graphical inset). The average glycerol contact *per residue* is significantly higher at the IC side (3.07 ± 1.46 compared to XC = 1.91 ± 0.63). This leaflet asymmetry with respect to glycerol contacts is also apparent in the CG simulations (cf. Supporting Information Figure S8D).

Lipid tail contact profiles for PC and PA are given in Supporting Information Figure S9E and Figure S8F, respectively. Aromatic residues make the most marked numbers of contacts with lipid chains, with similar residues as those identified from CG simulations, namely, Trp24, Phe141, Phe142, Tyr152, and Phe194 being especially prominent for both PC and PA. While there is no significant leaflet asymmetry with respect to tail contacts *per residue*, for PA (Supporting Information Figure S9F), there are higher numbers of contacts with aromatic residues at the IC leaflet, in agreement with CG simulations (cf. Supporting Information Figure S8F).

CONCLUSIONS

For membrane proteins, including gap junctional connexins, interactions with membrane lipids can exert dramatic functional consequences. Recent experimental work (*21*) has highlighted the importance of auxiliary lipid components such as (negatively charged) PA and cholesterol in facilitating channel activity. PA and other anionic lipids were also identified as tightly associated lipid species, lending support to the proposal that their specific interactions with proteins are a major contributory factor for the modulation of protein function. In this work, we have employed the coarse-grained MARTINI force field in conjunction with MD simulations to study the specific interactions between a Cx26 hemichannel and a number of lipid species, including PC, anionic

PA, and cholesterol, in order to identify sites at the protein interface which may exhibit preferential, specific binding to these lipids, as well as determine some of the main characteristics of these interactions.

Our CG simulation results suggest an enrichment of interfacial POPA at the intracellular leaflet at high bulk PA concentrations. We have determined that POPC and POPA can form especially tight binding interactions with the hemichannel at intersubunit crevices (classical nonannular sites). In mixed bilayers, however, POPA effectively competes with POPC for these sites, displacing the latter at some sites. We propose that occupation of nonannular sites by anionic lipids is sufficient to support channel function. Additionally, examination of the contacts between lipid headgroups and hemichannel residues indicates that the regions at the protein surface at which POPC and POPA binds are similar for the two lipids. This is also apparent by examination of the lipid density plots, which show that nonannular sites accommodate tightly bound POPC as well as POPA.

However, POPA exhibits a unique property of being capable of forming stable hydrophilic contacts with multiple residues spanning two different adjacent subunits at *both* leaflets of the bilayer, as opposed to POPC which can only do so at the extracellular side. These results suggest that POPA may be essential to channel function by helping to hold the protein together, especially at the intracellular side where there is an excess of positive charge at the protein (complementing the negative charge of POPA), enabling concerted motions between the subunits during the course of channel gating (pore opening/closing). Interestingly, Locke et al. (*21*) found that a relatively small number of POPA are required to support channel function; beyond this concentration (even up to 100%) no further significant alterations in channel function were observed. In our simulations, we show that at relatively low concentrations of POPA they migrate to and bind tightly at a discrete number of nonannular sites, especially at intersubunit crevice regions. It is possible that, once these sites are saturated by POPA (or other anionic lipids), channel function is already fully supported, with higher concentrations of anionic lipids making little further contribution. We note that the accumulation of tight-binding anionic lipids at the hemichannel interface may serve important roles in the voltage-sensitive gating of Cx26. Such a role has been proposed by Kocherginsky (*60*) for acidic lipids in voltage-sensitive sodium and potassium channels. Indeed, our simulations indicate that the composition of POPA is substantially enriched at the Cx26 interface relative to the bulk, especially at the intracellular leaflet. This interfacial enrichment may serve an important functional role in the voltage gating of the hemichannel.

A number of residues were identified which form high numbers of interatomic contacts with lipid headgroup components. These residues reside in lipid-exposed regions of the hemichannel surface and are qualitatively similar for both lipids. On the basis of these results, we propose that the biophysical consequences of mutations of certain residues which were identified as forming high contact numbers with lipid headgroups (e.g., loss of gap junction function) may at least be partially attributed to disruptions of Cx26−lipid interactions. Simulation of a mixed POPC:cholesterol bilayer suggests that the hemichannel enhances the transbilayer mobility of vicinal cholesterols, increasing the likelihood of site-hopping and interleaflet flip-flop transitions. These dynamical phenomena appear to be mediated by transient stabilizing interactions between cholesterol and the transmembrane domain of the protein. We have also performed atomistic simulations to investigate POPC and POPA interactions with Cx26 as comparisons with CG simulations and to provide further insights into additional interactions that may be present. These simulations revealed qualitative agreement with CG simulations with respect to the identities of the residues exposed to different lipid functional groups, as well as leaflet-dependent asymmetry in lipid contacts per residue.

ACKNOWLEDGMENT

We thank the Australian National Computational Infrastructure (NCI), Victorian Partnership for Advanced Computing (VPAC), and the Victorian Life Sciences Computation Initiative (VLSCI) for the generous provision of computational resources.

SUPPORTING INFORMATION AVAILABLE

Further information regarding simulation setup, trajectory-averaged data for individual subunits in each replicate simulation, contact lifetime histograms for replicate simulations, and lipid functional group average number of contacts with respect to residue. This material is available free of charge via the Internet at http://pubs.acs.org.

REFERENCES

1. Revel, J. P., Olson, W., and Karnovsk, Mj. (1967) A 20-angstrom gap junction with a hexagonal array of subunits in smooth muscle. *J. Cell Biol. 35*, A112.
2. Zampighi, G., Corless, J. M., and Robertson, J. D. (1980) On gap junction structure. *J. Cell Biol. 86*, 190–198.
3. Revel, J. P., Yancey, S. B., and Nicholson, B. J. (1986) The gap junction proteins. *Trends Biochem. Sci. 11*, 375–377.
4. Wei, C. J., Francis, R., Xu, X., and Lo, C. W. (2005) Connexin43 associated with an N-cadherin-containing multiprotein complex is required for gap junction formation in NIH3T3 cells. *J. Biol. Chem. 280*, 19925–19936.
5. Mese, G., Richard, G., and White, T. W. (2007) Gap junctions: Basic structure and function. *J. Invest. Dermatol. 127*, 2516–2524.
6. Loewenstein, W. R., Kanno, Y., and Socolar, S. J. (1978) Cell-to-cell channel. *Fed. Proc. 37*, 2645–2650.
7. Kanno, Y., and Loewenstein, W. R. (1966) Cell-to-cell passage of large molecules. *Nature 212*, 629.
8. Kanno, Y., and Loewenstein, W. R. (1964) Intercellular diffusion. *Science 143*, 959.
9. Kanno, Y., and Loewenstein, W. R. (1964) Low-resistance coupling between gland cells. Some observations on intercellular contact membranes + intercellular space. *Nature 201*, 194.
10. Lawrence, T. S., Beers, W. H., and Gilula, N. B. (1978) Transmission of hormonal-stimulation by cell-to-cell communication. *Nature 272*, 501–506.
11. Makowski, L., Caspar, D. L. D., Phillips, W. C., and Goodenough, D. A. (1977) Gap junction structures. 2. Analysis of X-ray diffraction data. *J. Cell Biol. 74*, 629–645.
12. Goodenough, D. A., and Paul, D. L. (2003) Beyond the gap: Functions of unpaired connexon channels. *Nat. Rev. Mol. Cell Biol. 4*, 285–294.
13. Kemperman, M. H., Hoefsloot, L. H., and Cremers, C. W. R. J. (2002) Hearing loss and connexin 26. *J. R. Soc. Med. 95*, 171–177.
14. Maeda, S., Nakagawa, S., Suga, M., Yamashita, E., Oshima, A., Fujiyoshi, Y., and Tsukihara, T. (2009) Structure of the connexin 26 gap junction channel at 3.5 angstrom resolution. *Nature 458*, 597–U561.
15. Lee, A. G. (2003) Lipid-protein interactions in biological membranes: A structural perspective. *Biochim. Biophys. Acta 1612*, 1–40.
16. Lee, A. G. (2004) How lipids affect the activities of integral membrane proteins. *Biochim. Biophys. Acta 1666*, 62–87.
17. Palsdottir, H., and Hunte, C. (2004) Lipids in membrane protein structures. *Biochim. Biophys. Acta 1666*, 2–18.
18. Sanderson, J. M. (2005) Peptide lipid interactions: Insights and perspectives. *Org. Biomol. Chem. 3*, 201–212.
19. Hunte, C., and Richers, S. (2008) Lipids and membrane protein structures. *Curr. Opin. Struct. Biol. 18*, 406–411.

20. Marsh, D. (2008) Protein modulation of lipids, and vice-versa, in membranes. *Biochim. Biophys. Acta 1778*, 1545–1575.
21. Locke, D., and Harris, A. L. (2009) Connexin channels and phospholipids: Association and modulation. *BMC Biol. 7*, 52–76.
22. Ash, W. L., Zlomislic, M. R., Oloo, E. O., and Tieleman, D. P. (2004) Computer simulations of membrane proteins. *Biochim. Biophys. Acta 1666*, 158–189.
23. Kandt, C., Ash, W. L., and Tieleman, D. P. (2007) Setting up and running molecular dynamics simulations of membrane proteins. *Methods 41*, 475–488.
24. Sapay, N., and Tieleman, D. P. (2008) Molecular dynamics simulation of lipid-protein interactions. *Curr. Top. Membr. 60*, 111–130.
25. Lindahl, E., and Sansom, M. S. P. (2008) Membrane proteins: Molecular dynamics simulations. *Curr. Opin. Struct. Biol. 18*, 425–431.
26. Deol, S. S., Domene, C., Bond, P. J., and Sansom, M. S. P. (2006) Anionic phospholipid interactions with the potassium channel KcsA: Simulation studies. *Biophys. J. 90*, 822–830.
27. Cheng, M. H., Xu, Y., and Tang, P. (2009) Anionic lipid and cholesterol interactions with alpha 4 beta 2 nAChR: Insights from MD simulations. *J. Phys. Chem. B 113*, 6964–6970.
28. Dickey, A. N., and Faller, R. (2008) Behavioral differences between phosphatidic acid and phosphatidylcholine in the presence of the nicotinic acetylcholine receptor. *Biophys. J. 95*, 5637–5647.
29. Khelashvili, G., Grossfield, A., Feller, S. E., Pitman, M. C., and Weinstein, H. (2009) Structural and dynamic effects of cholesterol at preferred sites of interaction with rhodopsin identified from microsecond length molecular dynamics simulations. *Proteins 76*, 403–417.
30. Lyman, E., Higgs, C., Kim, B., Lupyan, D., Shelleys, J. C., Farid, R., and Voth, G. A. (2009) A role for a specific cholesterol interaction in stabilizing the apo configuration of the human A(2A) adenosine receptor. *Structure 17*, 1660–1668.
31. Monticelli, L., Kandasamy, S. K., Periole, X., Larson, R. G., Tieleman, D. P., and Marrink, S. J. (2008) The MARTINI coarse-grained force field: Extension to proteins. *J. Chem. Theory Comput. 4*, 819–834.
32. Marrink, S. J., Risselada, H. J., Yefimov, S., Tieleman, D. P., and de Vries, A. H. (2007) The MARTINI force field: Coarse grained model for biomolecular simulations. *J. Phys. Chem. B 111*, 7812–7824.
33. Marrink, S. J., de Vries, A. H., and Mark, A. E. (2004) Coarse grained model for semiquantitative lipid simulations. *J. Phys. Chem. B 108*, 750–760.
34. Chetwynd, A. P., Scott, K. A., Mokrab, Y., and Sansom, M. S. P. (2008) CGDB: A database of membrane protein/lipid interactions by coarse-grained molecular dynamics simulations. *Mol. Membr. Biol. 25*, 662–669.
35. Sansom, M. S. P., Scott, K. A., and Bond, P. J. (2008) Coarse-grained simulation: A high-throughput computational approach to membrane proteins. *Biochem. Soc. Trans. 36*, 27–32.
36. Fleishman, S. J., Sabag, A. D., Ophir, E., Avraham, K. B., and Ben-Tal, N. (2006) The structural context of disease-causing mutations in gap junctions. *J. Biol. Chem. 281*, 28958–28963.
37. Fleishman, S. J., Unger, V. M., Yeager, M., and Ben-Tal, N. (2004) A C-alpha model for the transmembrane alpha helices of gap junction intercellular channels. *Mol. Cell 15*, 879–888.
38. Gunsteren, W. F. v., Billeter, S. R., Eising, A. A., Huenenberger, P. H., Krueger, P., Mark, A. E., Scott, W. R. P., and Tironi, I. G. (1996) Biomolecular Simulation: The GROMOS96 Manual and User Guide, vdf Hochschulverlag AG an der ETH Zürich and BIOMOS b.v., Zurich, Groningen.
39. Lindahl, E., Hess, B., and van der Spoel, D. (2001) GROMACS 3.0: A package for molecular simulation and trajectory analysis. *J. Mol. Model. 7*, 306–317.
40. Van der Spoel, D., Lindahl, E., Hess, B., Groenhof, G., Mark, A. E., and Berendsen, H. J. C. (2005) GROMACS: Fast, flexible, and free. *J. Comput. Chem. 26*, 1701–1718.
41. Berendsen, H. J. C., Postma, J. P. M., Vangunsteren, W. F., Dinola, A., and Haak, J. R. (1984) Molecular dynamics with coupling to an external bath. *J. Chem. Phys. 81*, 3684–3690.
42. Oostenbrink, C., Soares, T. A., van der Vegt, N. F. A., and van Gunsteren, W. F. (2005) Validation of the 53A6 GROMOS force field. *Eur. Biophys. J. 34*, 273–284.
43. Oostenbrink, C., Villa, A., Mark, A. E., and Van Gunsteren, W. F. (2004) A biomolecular force field based on the free enthalpy of hydration and solvation: The GROMOS force-field parameter sets 53A5 and 53A6. *J. Comput. Chem. 25*, 1656–1676.
44. Berger, O., Edholm, O., and Jahnig, F. (1997) Molecular dynamics simulations of a fluid bilayer of dipalmitoylphosphatidylcholine at full hydration, constant pressure, and constant temperature. *Biophys. J. 72*, 2002–2013.
45. Darden, T., York, D., and Pedersen, L. (1993) Particle mesh Ewald—An N.Log(N) method for Ewald sums in large systems. *J. Chem. Phys. 98*, 10089–10092.
46. Humphrey, W., Dalke, A., and Schulten, K. (1996) VMD: Visual molecular dynamics. *J. Mol. Graphics 14*, 33.
47. Guex, N., and Peitsch, M. C. (1997) SWISS-MODEL and the Swiss-PdbViewer: An environment for comparative protein modeling. *Electrophoresis 18*, 2714–2723.
48. Marrink, S. J., de Vries, A. H., Harroun, T. A., Katsaras, J., and Wassall, S. R. (2008) Cholesterol shows preference for the interior of polyunsaturated lipid. *J. Am. Chem. Soc. 130*, 10.
49. Risselada, H. J., and Marrink, S. J. (2008) The molecular face of lipid rafts in model membranes. *Proc. Natl. Acad. Sci.U.S.A. 105*, 17367–17372.
50. Kabsch, W., and Sander, C. (1983) Dictionary of protein secondary structure—Pattern recognition of hydrogen-bonded and geometrical features. *Biopolymers 22*, 2577–2637.
51. vanKlompenburg, W., Nilsson, I., vonHeijne, G., and deKruijff, B. (1997) Anionic phospholipids are determinants of membrane protein topology. *EMBO J. 16*, 4261–4266.
52. Jones, O. T., Eubanks, J. H., Earnest, J. P., and Mcnamee, M. G. (1988) A minimum number of lipids are required to support the functional properties of the nicotinic acetylcholine receptor. *Biochemistry 27*, 3733–3742.
53. Jones, O. T., and Mcnamee, M. G. (1988) Annular and nonannular binding-sites for cholesterol associated with the nicotinic acetylcholine receptor. *Biochemistry 27*, 2364–2374.
54. Arias, H. R. (1998) Binding sites for exogenous and endogenous non-competitive inhibitors of the nicotinic acetylcholine receptor. *Biochim. Biophys. Acta 1376*, 173–220.
55. Arias, H. R. (1997) Topology of ligand binding sites on the nicotinic acetylcholine receptor. *Brain Res. Rev. 25*, 133–191.
56. Dreger, M., Krauss, M., Herrmann, A., and Hucho, F. (1997) Interactions of the nicotinic acetylcholine receptor transmembrane segments with the lipid bilayer in native receptor-rich membranes. *Biochemistry 36*, 839–847.
57. Bennett, W. F. D., MacCallum, J. L., Hinner, M. J., Marrink, S. J., and Tieleman, D. P. (2009) Molecular view of cholesterol flip-flop and chemical potential in different membrane environments. *J. Am. Chem. Soc. 131*, 12714–12720.
58. Dinh, E. H., Ahmad, S., Chang, Q., Tang, W. X., Stong, B., and Lin, X. (2009) Diverse deafness mechanisms of connexin mutations revealed by studies using in vitro approaches and mouse models. *Brain Res. 1277*, 52–69.
59. Zachowski, A. (1993) Phospholipids in animal eukaryotic membranes—Transverse asymmetry and movement. *Biochem. J. 294*, 1–14.
60. Kocherginsky, N. (2009) Voltage-sensitive ion channels, acidic lipids and Hodgkin-Huxley equations: New ideas 55 years later. *J. Membr. Sci. 328*, 58–74.